7110 *Biochemistry* **2009,** *48,* 7110–7122
DOI: 10.1021/bi900745b

BIOCHEMISTRY
including biophysical chemistry & molecular biology
Article

Biophysical Investigation of GpIbα Binding to Thrombin Anion Binding Exosite II[†]

T. Michael Sabo and Muriel C. Maurer*

Department of Chemistry, University of Louisville, 2320 South Brook Street, Louisville, Kentucky 40292

Received April 30, 2009; Revised Manuscript Received June 23, 2009

ABSTRACT: Substrates and cofactors of the serine protease thrombin (IIa) employ two anion binding exosites (ABE-I and -II) to aid in binding. On the surface of platelets resides the GpIbα/β−GpIX−GpV membrane-bound receptor complex. IIa's ABE-II is proposed to interact with an anionic portion of GpIbα which enhances IIa cleavage of PAR-1 and subsequent activation of platelets. In this work, one-dimensional (1D) and two-dimensional (2D) NMR, analytical ultracentrifugation (AUC), and hydrogen−deuterium exchange (HDX) coupled with MALDI-TOF MS were performed to further characterize the features of binding to IIa's ABEs. The described work builds upon investigations performed in a prior study with fibrin(ogen)'s γ' peptide and IIa [Sabo, T. M., Farrell, D. H., and Maurer, M. C. (2006) *Biochemistry 45*, 7434−7445]. 1D line broadening NMR (^{1}H and ^{31}P) and 2D trNOESY NMR studies indicate that GpIbα residues D^{274}−E^{285} interact extensively with the IIa surface in an extended conformation. AUC demonstrates that both GpIbα (269−286) and γ' (410−427) peptides interact with IIa with a 1:1 stoichiometry. When the HDX results are compared to those for the ABE-I targeting peptide hirudin (54−65), the data imply that GpIbα (269−286), GpIbα (1−290), and γ' (410−427) are indeed directed to ABE-II. The ABE-II binding fragments reduce HDX for sites distant from the interface, suggesting long-range conformational effects. These studies illustrate that GpIbα and γ' target ABE-II with similar consequences on IIa dynamics, albeit with differing structural features.

At the nexus of procoagulation and anticoagulation resides the serine protease thrombin (IIa)[1] (*1*−*3*). The procoagulant activities of IIa are multifaceted and numerous, including the conversion of fibrinogen to fibrin to form the soft clot (*4*) and the activation of platelets through cleavage of the protease-activated receptors (PARs) (*5*). A vital anticoagulant function of IIa is the activation of protein C which deactivates several procoagulant enzymes (*6*). The specificity of IIa is a result of the loops and residues that surround the active site (*7*). IIa contains two electropositive patches that flank the catalytic site termed anion binding exosites I and II (ABE-I and ABE-II, respectively) (*8*). Exosites guide substrate orientation for catalysis that is more efficient and/or provide a separate cofactor interaction site that either enhances or dampens enzyme reactivity.

An important event in coagulation is the initial recruitment of IIa by glycoprotein Ibα (GpIbα) to the surface of platelets. This glycoprotein is part of the highly glycosylated GpIbα/β−GpIX−GpV transmembrane platelet receptor (*9*, *10*). The importance of this receptor is highlighted in Bernard-Soulier syndrome, a bleeding disorder resulting from either dysfunctional or low levels of this complex. GpIbα serves a multitude of functions that include binding coagulation proteins, adhering platelets to the site of damaged tissue, and aiding in leukocyte recruitment to combat infection. Two features of the N-terminus of GpIbα are a leucine rich repeat (LRR) domain and an anionic cluster (^{269}DEGDT-DLY$_S$DY$_S$Y$_S$PEEDTEG^{286}) (Table 1 and Figure 1A).

Considerable interest has been directed toward understanding in more detail the nature of the GpIbα−IIa interaction (*12*, *13*). Mutagenesis studies have identified ABE-II residues R^{93}, R^{97}, R^{101}, R^{233}, K^{236}, and K^{240} as playing a role in binding, not ABE-I residues R^{67}, R^{73}, R^{75}, R^{76}, and R^{77A} (*14*−*16*).[2] Additionally, the ABE-II binding glycosaminoglycan heparin prevents interaction of GpIbα with IIa (*15*). Conversely, others suggest ABE-I as GpIbα's binding site through competitive inhibition with hirudin (54−65) (*17*−*19*). Hirudin is a well-characterized ABE-I targeting IIa inhibitor isolated from the salivary glands of medicinal leeches (*20*). It should also be noted that GpIbα binding to IIa hinders the release of fibrinopeptide A (FpA) from fibrinogen (*14*, *21*, *22*), enhances PAR-1 hydrolysis (*23*), and decreases the level of catalysis at R^{372} in FVIII (*24*).

[†]Funding for this project was provided by National Institutes of Health Grant R01HL68440 (to M.C.M.).

*To whom correspondence should be addressed. Telephone: (502) 852-7008. Fax: (502) 852-8149. E-mail: muriel.maurer@louisville.edu.

[1]Abbreviations: IIa, thrombin; PAR-1, protease-activated receptor 1; ABE-I, anion binding exosite I; ABE-II, anion binding exosite II; GpIbα, glycoprotein Ibα; LRR, leucine rich repeat; FpA, fibrinopeptide A; FVIII, blood clotting factor VIII; PPACK, D-Phe-Pro-Arg chloromethyl ketone; Y_S, sulfotyrosine; Y_P, phosphotyrosine; NMR, nuclear magnetic resonance; 1D, one-dimensional; 2D, two-dimensional; TOCSY, total correlation spectroscopy; trNOESY, transferred nuclear Overhauser effect spectroscopy; PDB, Protein Data Bank; MALDI-TOF MS, matrix-assisted laser desorption ionization time-of-flight mass spectrometry; HDX, hydrogen−deuterium exchange; AUC, analytical ultracentrifugation; *S*, Svedberg constant; K_D, equilibrium binding constant.

[2]Throughout the paper, thrombin residues have been referenced according to the chymotrypsin numbering scheme.

 Published on Web 07/10/2009

Table 1: Peptides Utilized in IIa Binding Studies

GpIbα $\mathbf{Y_P}^{276}\mathbf{Y_P}^{278}\mathbf{Y_P}^{279}$	^{269}DEGDTDL$\mathbf{Y_P}$D$\mathbf{Y_P}\mathbf{Y_P}$PEEDTEG^{286}
GpIbα $\mathbf{Y_P}^{276}$Y$^{278}\mathbf{Y_P}^{279}$	^{269}DEGDTDL$\mathbf{Y_P}$DY$\mathbf{Y_P}$PEEDTEG^{286}
GpIbα Y^{276}Y^{278}Y^{279}	^{269}DEGDTDLYDYYPEEDTEG^{286}
γ' $\mathbf{Y_P}^{418}\mathbf{Y_P}^{422}$	^{410}PEHPAETE$\mathbf{Y_P}$DSL$\mathbf{Y_P}$PEDDL^{427}
hirudin $\mathbf{Y_S}^{63}$	^{54}GDFEEIPEE$\mathbf{Y_S}$LQ^{65}

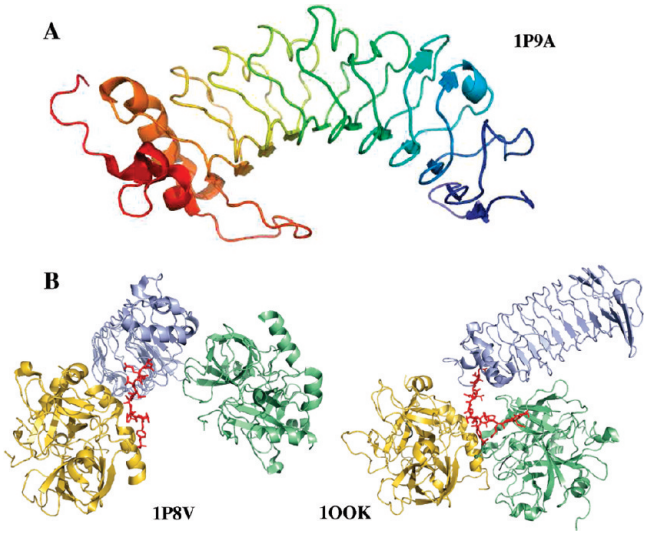

FIGURE 1: (A) Structure of glycoprotein Ibα (1−266) (PDB entry 1P9A) (*25*). The highly anionic C-terminal tail (269−286) is not modeled in this structure. The most prominent feature of the structure is the leucine rich repeat domain that forms the curvature of the protein. (B) Two views of GpIbα binding to thrombin. The crystal structures depict similar ABE-II interactions but differ in the depiction of thrombin dimerization. Colored blue is GpIbα, and the anionic C-terminal tail is colored red. Thrombin colored gold binds to the C-terminal tail, while thrombin colored green binds at different interfaces. The structure on the left is PDB entry 1P8V (*26*), and the structure on the right is PDB entry 1OOK (*27*). These figures were created using PyMol (*11*).

Two crystal structures of the IIa−GpIbα complex were published concurrently in 2003 (PDB entries 1OOK and 1P8V) (*25*, *26*) (Figure 1B). Though both groups reported a 1:1 asymmetric unit, symmetry-related molecules exhibit unique binding interfaces. Both structures illustrate similar interactions of GpIbα with ABE-II. 1OOK shows the C-terminus of GpIbα potentially dimerizing IIa through interactions with both exosites (*25*). In 1P8V, the second IIa molecule binds to GpIbα at the C-terminal end of the LRR domain (*26*). Two independent groups have analyzed the available experimental data and have concluded that the stronger interaction likely involves ABE-II and GpIbα residues L^{275}−Y$_S^{279}$, present in both structures (*12*, *13*).

Like GpIbα, fibrin(ogen) has been demonstrated to bind ABE-I (*27*) and ABE-II (*28*, *29*). The large soluble glycoprotein fibrinogen is a dimer comprised of three domains, $(A\alpha B\beta\gamma_A)_2$ (*4*, *30*). During coagulation, IIa conversion of fibrinogen to fibrin $(\alpha\beta\gamma_A)_2$ initiates formation of the noncovalently associated soft clot. The N-termini of the six polypeptides begin in the central E region, supplying a low-affinity ABE-I binding site (*27*). The C-termini of the polypeptides reach laterally from the E region to form the flanking D regions. The ABE-II binding γ' chain (*28*, *29*) is a variant of the γ_A chain with an insertion of 20 amino acids at the C-terminus (^{408}VRPEHPAETEY$_S$DSLY$_S$PEDDL^{427}) (*31*, *32*) (Table 1).

Between 7 and 15% of fibrinogen circulates as γ_A/γ' as opposed to γ_A/γ_A (*33*, *34*). The potential physiological consequences associated with elevated levels of γ_A/γ' remain unclear. Some research has suggested that an abundance of γ_A/γ' is linked to an increased incidence of cardiovascular disease (*33*, *35*). Conversely, two independent groups demonstrated that reduced levels of the γ' chain were indicative of a greater risk for deep vein thrombosis (*36*, *37*).

A previous report utilized nuclear magnetic resonance (NMR) and hydrogen−deuterium exchange (HDX) coupled with matrix-assisted laser desorption ionization time-of-flight mass spectrometry (MALDI-TOF MS) to focus on the details of the γ' peptide (410−427)−IIa ABE-II interaction (*38*). These experiments localized γ' peptide binding within ABE-II and detected perturbations in HDX within ABE-I, the autolysis loop, and the A chain. Many observations reported from the NMR results correlated extremely well with the subsequently reported X-ray structure of γ' peptide-bound IIa (*39*).

In the investigation presented here, the GpIbα−IIa interaction was examined in further detail. Because of the high degree of similarity between the IIa binding sequences of GpIbα and the γ' chain (Table 1), perhaps these anionic peptides share conformational features. NMR experiments demonstrate that the GpIbα peptide binds to IIa in an extended conformation, unlike the turn structure reported for the γ' peptide (*38*). In addition, these studies were undertaken to better define the IIa exosite(s) responsible for GpIbα interaction, as well as to examine whether GpIbα binding induces the same long-range allostery that is observed when the γ' peptide binds to IIa. The HDX results reveal that binding of both the GpIbα peptide (269−286) and fragment (1−290) to IIa's ABE-II alters the dynamics of IIa HDX analogous to the γ' peptide. Finally, analytical ultracentrifugation (AUC) was implemented to observe the behavior of IIa with GpIbα or the γ' peptide in solution.

MATERIALS AND METHODS

Synthetic Peptides and GpIbα Fragments. Bachem (King of Prussia, PA) synthesized peptides based on residues 269−286 of GpIbα (Table 1). SynPep (Dublin, CA) synthesized a peptide based on residues 410−427 of the human fibrinogen γ' chain variant (Table 1). For both peptides, phosphotyrosines (Y_P) were substituted for the naturally occurring sulfotyrosines (Y_S) without sacrificing binding affinity (*28*, *40*). Sigma-Aldrich and Bachem prepared the sulfonated hirudin fragment of residues 54−65 (Table 1). MALDI-TOF MS measurements on an Applied Biosystems Voyager DE-Pro mass spectrometer were used to verify peptide mass. The concentrations of the peptide were determined by quantitative amino acid analysis (AAA Service Laboratory, Boring, OR).

The GpIbα (1−290) 3Y$_S$ fragment (Y$_S^{276}$Y$_S^{278}$Y$_S^{279}$) and the GpIbα (1−290) 2Y$_S$ fragment (Y$_S^{276}$Y$_S^{279}$) were generous gifts from the Ruggeri Laboratory at Scripps Institute in La Jolla, CA. The procedure for *Drosophila melanogaster* expression and purification of the two GpIbα fragments is detailed in a previous report (*25*). To characterize the GpIbα fragments, MALDI-TOF MS was used to observe the mass of the proteins.

Use of Bovine Thrombin. Thrombin was purified from bovine plasma barium sulfate eluate (Sigma-Aldrich) as described by Trumbo and Maurer (*41*). It should be noted that human and bovine IIa exhibit a high degree of sequence conservation (87% identical) (*8*). Important regions where there are no differences include the active site, the Na^+ binding site, the β-insertion (W^{60D}) loop, and both ABEs.

The interaction of the human derived fibrin(ogen) γ' and GpIbα fragments with bovine IIa should not be influenced by the

minor differences between the species. Supporting this statement is an HDX study, in which PPACK inhibition of human and bovine IIa affected HDX in a similar manner for analogous peptides from both types of IIa (*42*). In addition, 2D trNOESY NMR experiments aimed at examining the structural features adopted by fibrinopeptide A (*43*, *44*) and a PAR1 peptide (*45*) bound to bovine IIa were in agreement with the corresponding human IIa X-ray structures (*46*, *47*). Finally, in the previous study concerning the γ' peptide and IIa, 2D trNOESY NMR results were similar for γ' peptide binding to both bovine α-IIa and human γ-IIa (*38*).

General Theory of ^1H and ^{31}P NMR. Sample preparation, $^1H/^{31}P$ NMR analysis, and NMR instrumentation were nearly identical to those described by Sabo et al. (*38*). The only difference is the exclusive use of the 500 MHz NMR spectrometer during the course of this work. A 1:10 ratio of enzyme (150 μM) to peptide (1.5 mM) was maintained for the three complexes studied: IIa−GpIbα ($Y_P^{276}Y_P^{278}Y_P^{279}$), IIa−GpIbα ($Y_P^{276}$-$Y_P^{279}$), and IIa−GpIbα (NoP). All complexes were examined at a pH of 5.6.

When free in solution, a peptide possesses very few secondary structural features because of a lack of constraining factors, such as a protein with which to interact (*48*, *49*). This situation results in an $\omega\tau_c$ value of $\approx$1 and longer transverse relaxation (T_2) times. The 1D spectrum will display very sharp peaks, and the 2D trNOESY spectrum will lack the presence of many discernible NOEs. Introduction of the binding partner, in this case IIa, leads to the peptide interacting with the protein. Thus, those protons that contact the protein surface adopt the solution characteristics of the larger macromolecule, i.e., $\omega\tau_c \gg 1$, shorter T_2 times, and large negative NOEs. The peptide now assumes the secondary conformational features associated with binding to the protein. If the k_{off} for the peptide is sufficiently fast, then the peptide will take a "memory" of the bound conformation to the free peptide population. This rejoining with the free peptide population results in 1D line broadening for protons that contact the protein surface and a weighted average of the NOEs of the free and bound ligands in the 2D trNOESY spectrum.

Analytical Ultracentrifugation. IIa was inhibited with a 2-fold excess of PPACK for 30 min. An assay involving the chromogenic substrate S2238 was employed to ensure that IIa was inactive. The PPACK−IIa complex was then subjected to overnight dialysis with 150 mM NaCl and 25 mM phosphate (pH 7.4). The γ' or GpIbα peptide was lyophilized and reconstituted in the same buffer. A series of sedimentation velocity AUC experiments ranging from 1, 2, 5, 10, and 20 times peptide to IIa (4.5−7.0 μM) in duplicate was performed in an XL-A AUC instrument (Beckman-Coulter). The parameters for each run were 60000 rpm, 25 °C, and 280 nm. The data were analyzed with DC-DT+.

HDX Sample Preparation. IIa was buffer exchanged into HDX buffer [37.5 mM NaCl and 6.25 mM NaH_2PO_4 (pH 5.6, 6.5, or 7.5) (all pH values are within ±0.1)] with an Amicon-Ultra 4 unit (10 kDa molecular mass cutoff). The concentration of IIa for all preparations was 25 μM. An aliquot of 24 μL of IIa and 24 μL of HDX buffer was evaporated to dryness using a SpeedVac unit (Savant). The dry aliquots were stored at −70 °C.

For experiments involving peptides, enough GpIbα, γ', or hirudin (54−65) was added to 24 μL of buffer-exchanged IIa to achieve a 20:1 ratio (40:1 in the case of the γ' peptide at pH 6.5) during HDX. The pHs of the peptides were adjusted prior to addition. The aliquots of buffer-exchanged IIa and peptide were evaporated to dryness using a SpeedVac unit. For experiments involving the proteins GpIbα-$3Y_S$ and GpIbα-$2Y_S$, the two fragments were exchanged into the pH 6.5 HDX buffer. After the buffer exchange, the GpIbα fragment concentration was 40 μM. An aliquot of 24 μL of IIa and 24 μL of GpIbα fragment was evaporated to dryness using a SpeedVac unit. The dry aliquots were stored at −70 °C.

The increased γ' (410−427) peptide to IIa ratio raises the possibility of discrepancies between results presented in an earlier report (*38*) and those described within this paper. Reanalysis of the γ' (410−427)−IIa HDX pH showed that the value was likely below 6.0 in the prior work compared to IIa HDX at pH 6.5 (*38*). The acidity of the γ' peptide stock solution surpassed the buffering capabilities of the 25 mM phosphate solution. Thus, both ABE-II binding and pH-dependent HDX rate perturbations were observed (*38*). When the pH of the γ' (410−427)−IIa solution was increased to 6.5 in our work, the residence time on the enzyme surface may have decreased. Increasing the peptide:IIa ratio to 40:1 promoted the observation of a single population of ligand-bound IIa. Fortuitously, the carefully monitored pH investigations described in this report validate the conclusions obtained in the previous study for the γ' (410−427)−IIa complex. Ligand binding to ABE-II decreases the level of HDX at the binding interface, which leads to further decreases in the level of HDX in regions not associated with the interaction site.

HDX Experiments. Dry aliquots were allowed to come to room temperature before the experiment was begun. First, 12 μL of D_2O was added to the dry aliquot, yielding the final concentrations: 50 μM IIa, 80 μM GpIbα fragment or 1−2 mM peptide, 150 mM NaCl, and 25 mM NaH_2PO_4 (pH 5.6, 6.5, or 7.5). The samples were incubated in a desiccator at room temperature for 1 or 10 min. After incubation, 114 μL of 0.1% TFA (pH 2.5, on ice) was added to quench the reaction. An additional 1 μL of 5% TFA was added to ensure that the pH was 2.5 in experiments conducted at pH 7.5. Next, 66 μL of the quenched solution was transferred to a tube of activated pepsin bound to agarose. Digestion occurred on ice for 10 min. Centrifugation at 4 °C separated the digest from the pepsin, and 8.2 μL aliquots were immediately frozen in liquid N_2. Each frozen HDX aliquot was analyzed as detailed by Sabo et al. with MALDI-TOF MS (*38*).

Coverage exists for 10 peptides in bovine IIa from a nonreducing pepsin digest (*42*). Figure 2 depicts the location of the 10 peptides within IIa relative to the two ABEs. Residues 65−84 represent a portion of ABE-I, while part of ABE-II is covered with three fragments: residues 85−99, 173−180, and 173−181. The autolysis loop peptide (135−149D) and residues 46−52 reside near ABE-I residues 65−84. A β strand within the segment of residues 106−116 is located antiparallel to a β strand near the N-terminus of ABE-II residues 85−99. A chain residues −13 to −4 of bovine IIa are highly flexible but when present in an X-ray structure [such as PDB entry 2A1D (*50*)] reach toward the C-terminal helix of the B chain (233−240), which has several ABE-II residues. Lastly, the segment of residues 202−207 fits into the hinge formed by the boomerang-shaped A chain.

The HDX experiments described in Results cover three topics: (1) the effect of pH on IIa HDX, (2) perturbations in IIa HDX due to peptide binding at pH 5.6 and 6.5, and (3) a comparison of GpIbα peptide and GpIbα protein binding to IIa at pH 6.5. The data will be reported in two ways. Raw HDX will be illustrated in a 1 and 10 min bar graph for the four topics (Figures 6 and 8−10) (*38*). In addition, the numerical values have been reported in Tables 1 and 2 of the Supporting Information. The second

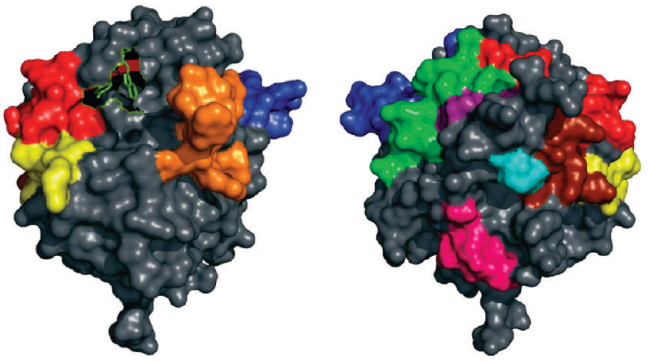

FIGURE 2: Depiction of the coverage obtained from a peptic digest of IIa (PDB entry 2AID) relative to Y^{60A} and W^{60D}, which are colored green: (left) looking onto the active site of IIa and (right) structure rotated 180° about the *y*-axis. Peptides from the peptic digest are colored as follows: the ABE-II regions of residues 85−99 (red) and 173−181 (yellow), ABE-I peptide 65−84 (blue), autolysis loop containing peptide 135−149D (orange), 106−116 (green), A chain peptide of residues −13 to −4 (cyan), 202−207 (pink), and 46−52 (purple). The additional ABE-II region not observed in this HDX study, residues 233−240, is colored brown.

method of analysis employs percent changes to gauge the significance in fluctuations of HDX (Tables 3 and 4) (*38*). This value relates the differences in HDX to the theoretical maximum amount of exchangeable protons present in each observable peptide. These percent changes will be classified into three categories: (1) insignificant (0 to ±1.9%), (2) modest change (±2.0 to ±4.4%), and (3) significant change (greater than or equal to ±4.5%) (*38*, *51*−*54*).

RESULTS

^1H and ^{31}P One-Dimensional Line Broadening NMR. 1D NMR experiments were performed to determine which ^1H or ^{31}P nuclei within the GpIbα (269−286) peptide interact with IIa. The first set of 1D NMR spectra examined GpIbα ($Y_P^{276}Y_P^{278}Y_P^{279}$) and displayed the absence of significant line broadening for the peptide in the presence of IIa (data not shown). These findings indicate that the $3Y_P$ peptide binds too tightly to IIa, hindering any transfer of information regarding bound structural features to the free peptide population.

Since the GpIbα ($Y_P^{276}Y_P^{278}Y_P^{279}$) peptide spectra did not display line broadening, a $2Y_P$ variant was synthesized. The GpIbα ($Y_P^{276}Y_P^{279}$) peptide still interacts with IIa [demonstrated by the two crystal structures (*25*, *26*)], but the absence of one Y_P may sufficiently weaken the interaction for the appearance of 1D line broadening. The spectra in Figure 3A,B focus on the amide region and do illustrate some line broadening in the presence of IIa. Most of the broadening encompasses residues D^{274}−Y_P^{279}, while a modest amount is observed for residues E^{281}−D^{283}. However, the line broadening is not extensive, with residues D^{269}−D^{274} and T^{284}−G^{286} appearing unchanged from the free peptide spectrum. Curiously, the ^{31}P spectra do not present evidence of line broadening (data not shown).

A final peptide was synthesized without Y_P. Much more line broadening is evident with GpIbα (No Y_P) (Figure 3C,D). The central portion of the peptide spanning D^{274}−Y^{279}, E^{281}, and D^{283} displays a significant amount of line broadening. Residues E^{282} and E^{285} show a modest amount of broadening. Finally, N-terminal residues D^{269}−T^{273} and C-terminal residues T^{284} and G^{286} do not appear to be essential for the interaction of GpIbα (269−286) with IIa.

Table 2: Analytical Ultracentrifugation Data

	sedimentation coefficient (S)	molecular mass (kDa)
IIa alone	3.11 ± 0.00	36.2 ± 0.3
1:1 GpIbα:IIa	3.19 ± 0.02	37.3 ± 0.0
2:1 GpIbα:IIa	3.18 ± 0.01	37.5 ± 0.9
5:1 GpIbα:IIa	3.27 ± 0.05	37.9 ± 0.7
10:1 GpIbα:IIa	3.25 ± 0.02	37.2 ± 1.1
20:1 GpIbα:IIa	3.22 ± 0.01	38.1 ± 1.4
1:1 γ′:IIa	3.19 ± 0.02	39.3 ± 1.0
2:1 γ′:IIa	3.22 ± 0.03	38.6 ± 0.4
5:1 γ′:IIa	3.23 ± 0.03	39.9 ± 0.2
10:1 γ′:IIa	3.27 ± 0.01	39.9 ± 0.6
20:1 γ′:IIa	3.28 ± 0.01	40.9 ± 0.7

Table 3: Changes in Percent Deuteration for GpIbα−IIa and γ′ Peptide−IIa Complexes at 1 and 10 min Relative to IIa at pH 5.6[a]

	20:1					
	GpIbα		γ′		hirudin	
residues	1 min	10 min	1 min	10 min	1 min	10 min
−13 to −4	**−11.4**[b]	**−8.5**	**−5.2**	**−8.0**	**−4.9**	**−6.1**
46−52	−0.2	−1.5	−0.5	−1.4	−1.1	−1.4
65−84	**−11.5**	**−9.3**	**−6.9**	**−8.7**	**−21.4**	**−28.5**
85−99	**−11.1**	**−20.1**	**−9.4**	**−16.0**	−2.0	−3.4
106−113	−3.1	**−6.0**	−3.3	**−6.1**	−1.3	−0.1
106−116	−2.2	**−4.6**	−2.4	**−5.1**	−2.1	−0.9
135−149D	**−7.3**	**−5.6**	−4.0	**−7.5**	**−11.7**	**−13.5**
173−180	**−4.7**	**−12.7**	−3.7	**−11.2**	−4.0	−4.4
173−181	−4.4	**−11.5**	−3.8	**−10.6**	−3.8	−4.1
202−207	**−12.5**	**−17.9**	**−8.8**	**−10.0**	−2.8	**−7.4**

[a] The percent change for a particular peptide is calculated as described in ref *38*. [b] The values in bold represent significant changes in deuteration of more than −4.5%.

Two-Dimensional Transferred Nuclear Overhauser Effect NMR. The 2D spectrum of GpIbα ($Y_P^{276}Y_P^{278}Y_P^{279}$) was indistinguishable from the spectrum with the peptide in the presence of IIa (data not shown). For the $Y_P^{276}Y_P^{279}$ and No Y_P GpIbα peptides, the 2D trNOESY spectra displayed only nearest-neighbor NOEs in the presence of IIa. Figure 4 illustrates some of the key features from the GpIbα (No Y_P)−IIa 2D trNOESY spectra. Detection of only nearest-neighbor NOEs suggests that the peptide adopts an extended conformation when binding to IIa. In addition, the Y^{279}−P^{280} amide bond is in the *trans* conformation. With the GpIbα ($Y_P^{276}Y_P^{279}$) peptide, slightly fewer inter-residue NOEs are observed in the presence of IIa when compared to the number with GpIbα (No Y_P).

Analytical Ultracentrifugation. Two X-ray studies offer evidence of potential ABE-II binding ligand-induced IIa dimerization (*25*, *39*). AUC experiments were performed to monitor the behavior of IIa in the presence of the GpIbα or γ′ peptide. In these AUC trials, the concentrations of PPACK-inhibited IIa ranged from 4.7 to 7.0 μM. The sedimentation velocity experiments were executed with a range of peptide:IIa molar ratios varying from 0:1 to 20:1. Table 2 presents the data for the average of two runs. Figure 5 displays the distribution of Svedberg constants (*S*) for the trial examining a 2:1 GpIbα peptide:IIa ratio. This figure is representative of all data collected from 1:1 to 20:1 peptide:IIa ratios reported in Table 2.

The Svedberg constant measures the rate of sedimentation, which is related to the size and shape of the molecule (*55*). When

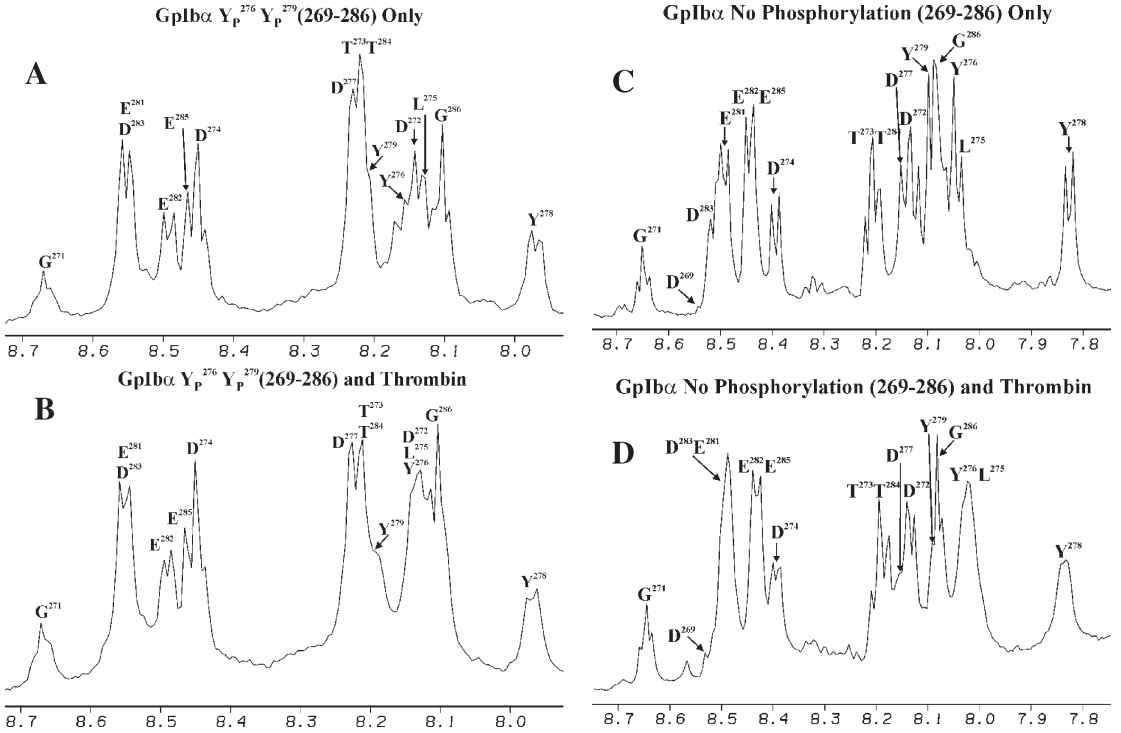

FIGURE 3: Line broadening spectra for the GpIbα peptides in the presence of thrombin. All NMR samples are in 25 mM H_3PO_4, 150 mM NaCl, 200 μM EDTA, and 10% D_2O (pH 5.6). (A) 1D NMR spectrum for 1.5 mM $Y_P^{276}Y_P^{279}$ peptide in solution. (B) 1D NMR spectrum for 1.5 mM $Y_P^{276}Y_P^{279}$ peptide in the presence of 0.15 mM IIa. The amide protons that display the most line broadening are D^{274}–Y_P^{279}. A moderate amount of line broadening is evident for the NH groups of residues E^{281}–D^{283}. Line broadening is not observed for the amide protons of residues D^{269}–T^{273} and T^{284}–G^{286}. (C) 1D NMR spectrum for 1.5 mM unphosphorylated peptide in solution. (D) 1D NMR spectrum for 1.5 mM unphosphorylated peptide in the presence of 0.15 mM IIa. The amide protons that display the most line broadening are those of residues D^{274}–Y_P^{279}, E^{281}, and D^{283}. A moderate amount of line broadening is evident for the NH groups of E^{282} and E^{285}. Line broadening is not observed for the amide protons of D^{269}–T^{273}, T^{284}, and G^{286}.

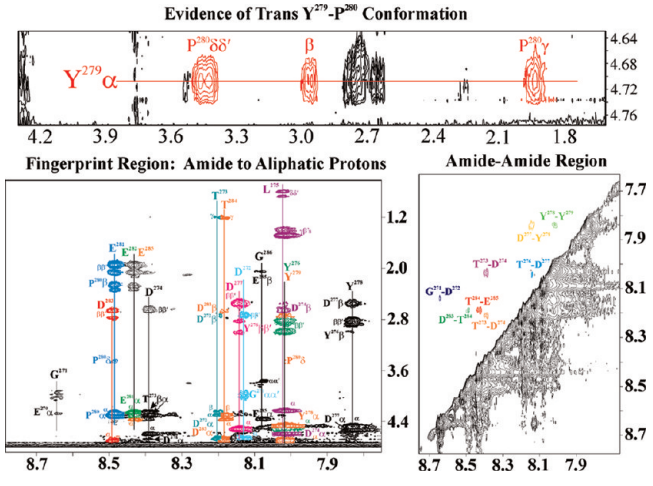

FIGURE 4: 2D trNOESY spectrum of the unphosphorylated GpIbα (1.5 mM) bound to IIa (0.15 mM). The top panel illustrates the evidence for a trans Y^{279}–P^{280} peptide bond. The bottom panels demonstrate that GpIbα exists in an extended structure when bound to IIa due to the presence of only nearest-neighbor NOEs. The NOEs are color-coded according to the corresponding residue.

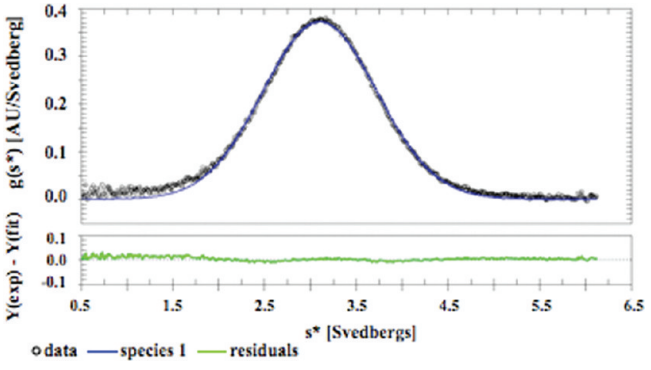

FIGURE 5: Sedimentation velocity AUC of GpIbα peptide (14 μM) and IIa (7 μM). Analysis was performed at 280 nm, 20 °C, and 60000 rpm in 150 mM NaCl and 25 mM phosphate (pH 7.4). The apparent Svedberg constant distribution centered at 3.2 S with the residuals resulting from a global fit of the data using DC-DT+.

two proteins interact, the surface area is decreased leading to a nonadditive increase in the *S* constant. The calculated Svedberg constants for the peptide binding to the enzyme range from 3.2 to 3.3, compared to 3.1 for IIa alone. The slight increase in molecular mass and *S* values with an increase in peptide concentration indicates that the peptides bind to IIa but do not instigate protein dimerization under these conditions.

HDX Experiments. (i) Observing the Effect of pH on Thrombin's Backbone Amide Solvent Accessibility. The HDX method exploits differences in the rate of chemical exchange for backbone amide protons in proteins (*56*). Surface-exposed backbone amide protons are more available for HDX than protons buried within the interior of the protein. Through fluctuations in protein structure (temporary protein unfolding and/or local conformational changes), a buried backbone amide proton may become exposed to solvent (*57*, *58*). Therefore, protein dynamics influence deuterium exchange to a great degree. The rate of chemical exchange is highly dependent on pH and temperature (*59*).

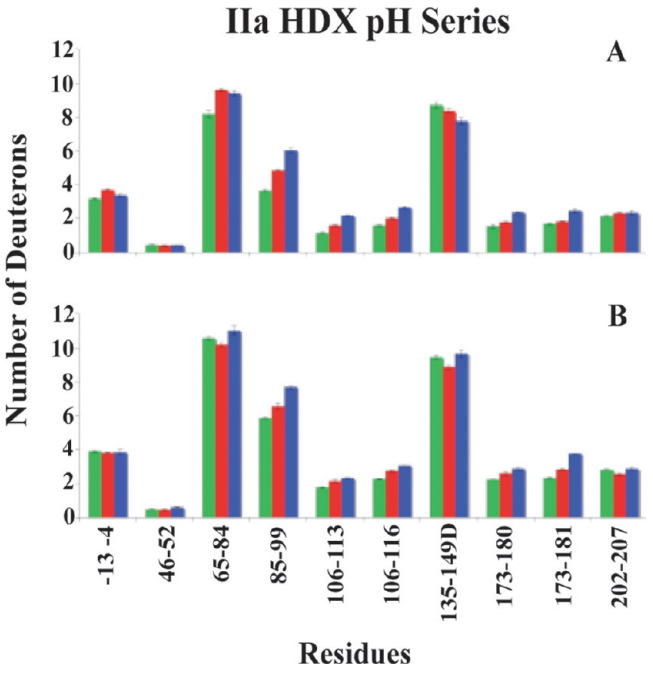

FIGURE 6: Graphs of deuterium incorporation for IIa at pH 5.6 (green), pH 6.5 (red), and pH 7.5 (blue): (A) HDX for 1 min and (B) HDX for 10 min. Errors correspond to the standard deviation of the mean for three independent experiments.

For this work, HDX effects at pH values of 5.6, 6.5, and 7.5 were examined. Work at pH 5.6 allows comparisons to be made with the NMR solution conditions. A pH of 7.5 is physiological, but the backbone amides exchange very rapidly. A more favorable working pH is 6.5, a condition that slows the backbone exchange 10-fold relative to that at pH 7.5 (*60*) and decreases the rate of IIa autolysis. Figure 2 illustrates the coverage obtained from a peptic digest of IIa (see Materials and Methods for a description).

Comparing the levels of HDX across this pH spectrum reveals three distinct groups (see Figure 6 and Tables 1 and 2 of the Supporting Information). The first grouping concerns those fragments that steadily increase in their level of deuterium incorporation as the pH increases, suggesting a significant degree of solvent exposure for some of the amide protons. These peptides include ABE-II peptides 85−99 and 173−181, as well as peptide 106−116. The second grouping involves peptides −13 to −4, 46−52, and 202−207. These three peptides seem impervious to pH change. Two probable explanations are that most of the amide protons are solvent inaccessible and/or the amide protons exchange too quickly for any apparent pH effect to be noticed. Finally, both ABE-I peptide 65−84 and autolysis loop 135−149D show stagnant levels of HDX at 10 min. At 1 min, an increase in pH appears to slow HDX for the autolysis loop peptide, perhaps indicating a more stable configuration for peptide 135−149D at higher pH. As for peptide 65−84, the rate of deuterium incorporation may slightly increase with a higher pH after HDX for 1 min.

(ii) Observing the Effect of the GpIbα ($Y_P^{276}Y_P^{278}$-Y_P^{279}) Peptide, the γ′ Peptide ($Y_P^{418}Y_P^{422}$), and Hirudin (54−65) on Thrombin's Backbone Amide Solvent Accessibility at pH 5.6 and 6.5. The first reports describing HDX coupled with MALDI-TOF MS to study solvent accessibility at a ligand−protein interface appeared in 1998 (*61*, *62*). With such an HDX experiment, the ligand should be bound to the protein, ideally, for the entire course of the deuterium exchange (*61*, *63*). Thus, the K_D describing the strength of the ligand−protein interaction, as well as the concentration of the binding partners, will determine the lifetime of the complex (*63*).

The GpIbα, γ′, and hirudin (54−65) peptides were incubated with IIa at room temperature and pH 5.6 or 6.5 for 1 or 10 min in the presence of 99.99% D_2O. A previous study found that GpIbα residues 265−285 bound to IIa with a K_D of 5.9 nM (*21*). In addition, the larger GpIbα fragment of residues 1−282 possesses a K_D of 149 nM (*64*). The weaker K_D may stem from the truncated C-terminus. For the sake of comparison, an ABE-I targeting peptide was also examined. Sulfonated hirudin (54−65) has a K_D of 48 nM, recently determined via fluorescence studies (*65*). Thus, 1 mM GpIbα and 1 mM hirudin (54−65) should provide 99.99% occupancy of 50 μM IIa. As for the γ′ peptide, the interaction is weaker (K_D = 680 nM) (*28*), resulting in 99.93 and 99.97% occupancy at 1 and 2 mM peptide, respectively.

In Figure 7, the isotopic cluster for residues 85−99 for a 20:1 γ′ peptide:IIa ratio at pH 6.5 has an interesting feature not evident at pH 5.6. The cluster appears to be expanded with a slight shoulder ending near *m*/*z* 2115 (not shown is a similar shoulder for residues 173−181). The results suggest the presence of two different IIa populations at pH 6.5 exposed to deuterium. HDX performed at pH 6.5 with a higher ratio (40:1) of the γ′ peptide (2 mM) to IIa (50 μM) led to the reappearance of a single isotopic cluster (see Materials and Methods for an explanation). Therefore, pH 6.5 HDX comparisons will be made among 20:1 hirudin (54−65):IIa, 20:1 GpIbα:IIa, and 40:1 γ′ peptide:IIa ratios.

The HDX results for peptide binding to IIa are compiled in Tables 3 and 4, Tables 1 and 2 of the Supporting Information, and Figures 8 and 9. After HDX for 1 and 10 min, both the GpIbα and γ′ peptides significantly protect ABE-II fragment 85−99 from deuterium. A unique feature of the data at pH 5.6 is the observed increase in the level of HDX protection at 10 min for 85−99, either indicating a tighter complex at the lower pH or representing the slower rate of HDX at this pH. Another segment within ABE-II, residues 173−181, increases in protection from 1 to 10 min of HDX at both pH values in a similar manner. These results suggest that the GpIbα and γ′ peptides are interacting with IIa's ABE-II. Conversely, hirudin (54−65) exclusively targets ABE-I which is evident from the dramatic HDX protection at residues 65−84.

Binding to ABE-I and ABE-II appears to protect regions within IIa unaffiliated with their interactive sites. Interactions of hirudin (54−65) with IIa lead to mostly modest decreases in the level of HDX for ABE-II peptides 85−99 and 173−181 over the course of 10 min. ABE-I fragment 65−84 is affected by GpIbα and γ′ binding to ABE-II to a greater degree than hirudin (54−65) ABE-I binding imparts to ABE-II. After HDX for 1 or 10 min at pH 5.6, fragment 65−84 displays slightly less deuterium incorporation with the GpIbα peptide than the γ′ peptide. At pH 6.5, interactions of the peptide with ABE-II show a large degree of protection at 1 min for 65−84 that becomes significantly reduced within 10 min.

Located parallel to a portion of ABE-II fragment 85−99 are residues 106−116 that are represented by two overlapping fragments. Hirudin (54−65) binding has very little effect on HDX for residues 106−116 at pH 5.6, but at pH 6.5, noteworthy protection can be localized to residues 106−113. Both the GpIbα and γ′ peptides display modest protection at 1 min, increasing to a level of greater significance at 10 min for experiments conducted

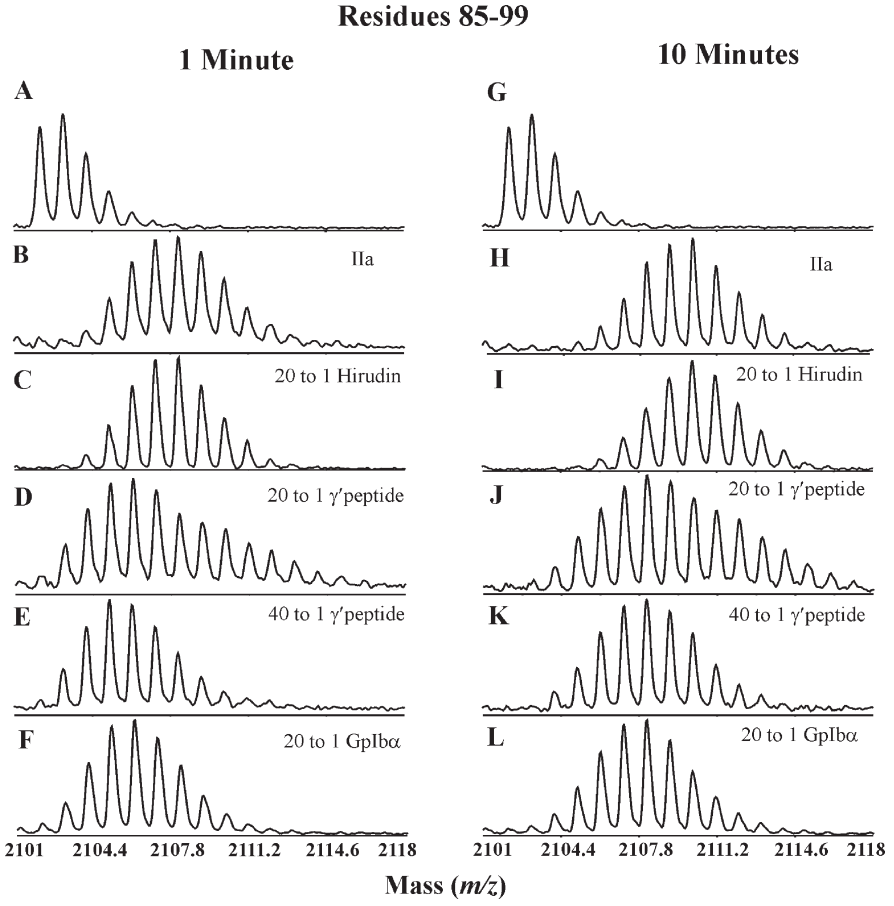

FIGURE 7: Mass spectra of residues 85−99 after HDX for 1 and 10 min. All of the depicted HDX experiments were conducted with 50 μM IIa in 150 mM NaCl and 25 mM NaH_2PO_4 (pH 6.5): (A and G) the undeuterated peak cluster, (B and H) IIa spectra in the absence of ligands, (C and I) 20:1 hirudin (54−65):IIa ratio, (D and J) 20:1 γ' peptide:IIa ratio, (E and K) 40:1 γ' peptide:IIa ratio, and (F and L) 20:1 GpIbα peptide:IIa ratio. At a ratio of 20:1, both the γ' and GpIbα peptides exhibit a similar degree of protection for these ABE-II residues; however, in spectra D and J, a small shoulder is present which suggests the presence of two IIa populations. Increasing the amount of γ' peptide completely abrogates the shoulder, suggesting fully occupied ABE-II.

at pH 5.6. As for pH 6.5, the levels of significant HDX protection remain steady from 1 to 10 min for residues 106−116. These data imply that ABE-II binding is transmitted to this neighboring β-strand.

Near ABE-I is segment 135−149D, which also encompasses most of the autolysis loop. All three peptides significantly slow HDX for this region of IIa. Hirudin (54−65) has a larger effect on the dynamics of this region from ABE-I than the GpIbα and γ' peptides from ABE-II. Another long-range consequence of ABE-I and ABE-II occupation is evident from HDX within the A chain residues −13 to −4 and nearby B chain fragment 202−207. The degree of protection is larger in magnitude for γ' and GpIbα, equating to mostly significant deviations from the HDX of IIa alone. Hirudin (54−65) results indicate that pH plays a role in HDX for residues −13 to −4 and 202−207. A higher pH of 6.5 results in these two peptides remaining largely unaffected by hirudin (54−65) binding to ABE-I, whereas at pH 5.6, significant protection is observed. All three peptides do not change the dynamics of deuterium exchange for fragment 46−52.

(iii) Observing the Effect of the GpIbα ($Y_P^{276}Y_P^{278}$-Y_P^{279}) Peptide and the GpIbα Fragment (1−290) on Thrombin's Backbone Amide Solvent Accessibility at pH 6.5. The Ruggeri laboratory at Scripps generously donated expressed GpIbα (1−290) with $3Y_S$ ($Y_S^{276}Y_S^{278}Y_S^{279}$) and $2Y_S$ ($Y_S^{276}Y_S^{279}$) with the goal of comparing the HDX of the peptide to a larger protein fragment. The GpIbα (1−290)−IIa HDX data recorded at pH 6.5 are quite similar for the $3Y_S$ protein and the $3Y_P$ peptide (Figure 10, Table 4, and Table 1 of the Supporting Information). The $2Y_S$ protein displayed similar trends in HDX; however, the degrees of percent change are not as large as with the $3Y_S$ protein. As with the two ABE-II binding peptides, the GpIbα (1−290) fragment appears to be interacting at ABE-II. Also, long-range HDX perturbations are evident toward ABE-I, the A chain, and the autolysis loop. It must be noted that the HDX results for hirudin (54−65) and GpIbα (1−290) are not similar. These findings further support the notion that GpIbα's primary destination on IIa is ABE-II.

DISCUSSION

On the surface of platelets, the receptor GpIbα forms a complex with IIa; however, the literature presents evidence for interactions at both ABEs. Though mutagenesis data strongly suggest that GpIbα binds exclusively at ABE-II (*14*−*16*), binding studies reveal interactions at both exosites (*15*, *17*, *19*, *21*, *64*). Adding to the ambiguity, two crystal structures of the GpIbα−IIa complex illustrate similar interactions at ABE-II for one IIa, while symmetry-related IIa binds to GpIbα through ABE-I at different GpIbα interfaces (*25*, *26*) (Figure 1B). The studies described in this report use solution NMR, AUC, and HDX coupled with MALDI-TOF MS to investigate the interaction of GpIbα with IIa.

Analysis of the NMR Data: The GpIbα Peptide (269−286) Binds to Thrombin in an Extended Conformation. To

Table 4: Changes in Percent Deuteration for Peptide and Protein Binding to IIa at 1 and 10 min Relative to Free IIa at pH 6.5[a]

	20:1				40:1		1.6:1			
	hirudin		GpIbα		γ′		GpIbα 3S		GpIbα 2S	
residues	1 min	10 min	1 min	10 min	1 min	10 min	1 min	10 min	1 min	10 min
−13 to −4	−3.5	1.2	**−12.8**	−3.2	**−15.8**	**−7.6**	**−14.8**	**−5.4**	**−8.5**	−1.2
46−52	−0.2	0.3	0.0	−0.6	−0.3	−0.6	−0.2	−0.6	−1.4	−0.3
65−84	**−24.9**[b]	**−18.6**	**−15.6**	−4.3	**−19.9**	**−8.9**	**−13.2**	−3.9	**−7.7**	−2.7
85−99	−3.6	2.0	**−13.7**	**−12.1**	**−13.1**	**−10.2**	**−13.0**	**−10.3**	**−8.0**	**−7.2**
106−113	**−5.8**	0.1	**−8.4**	**−7.0**	**−7.9**	**−6.1**	n/a	n/a	n/a	n/a
106−116	−4.1	−0.3	**−6.7**	**−6.6**	**−6.2**	**−5.6**	−2.6	−3.6	−2.6	−2.6
135−149D	**−5.0**	**−7.1**	**−5.5**	−3.6	n/a	n/a	**−4.8**	−4.4	**−4.8**	**−4.8**
173−180	**−5.1**	−2.2	**−5.4**	**−11.9**	**−7.8**	**−11.5**	n/a	n/a	n/a	n/a
173−181	−1.6	−1.1	**−5.5**	**−14.0**	**−8.4**	**−13.0**	**−7.0**	**−11.6**	**−7.0**	**−10.6**
202−207	−1.0	−1.2	**−4.7**	−1.9	**−7.6**	−2.5	n/a	n/a	n/a	n/a

[a] The % change for a particular peptide is calculated as described in (*38*). [b] The values in bold represent significant changes in deuteration of greater than −4.5%.

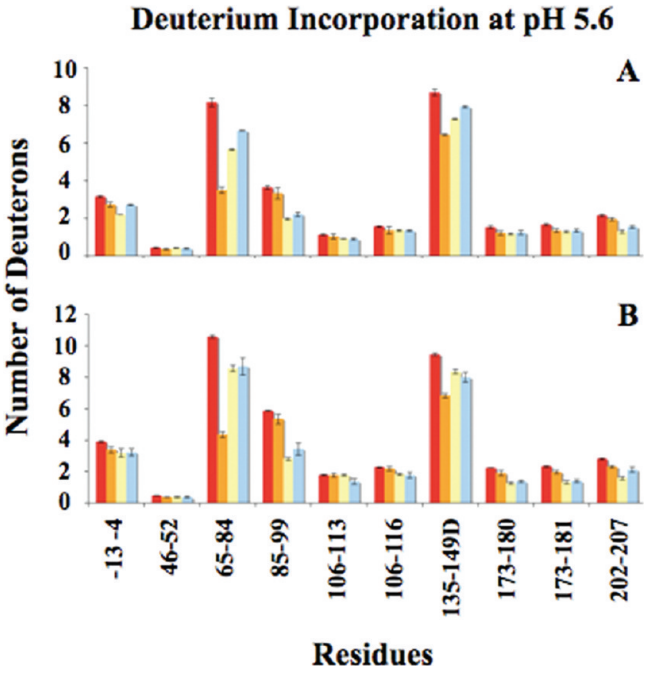

FIGURE 8: Graphs of deuterium incorporation for IIa and 20:1 peptide−IIa complexes at pH 5.6: (A) HDX for 1 min and (B) HDX for 10 min. The bars in the graph correspond to IIa alone (red) and hirudin−IIa (orange), GpIbα−IIa (yellow), and γ′ peptide−IIa (blue) complexes. Errors correspond to the standard deviation of the mean for three independent experiments.

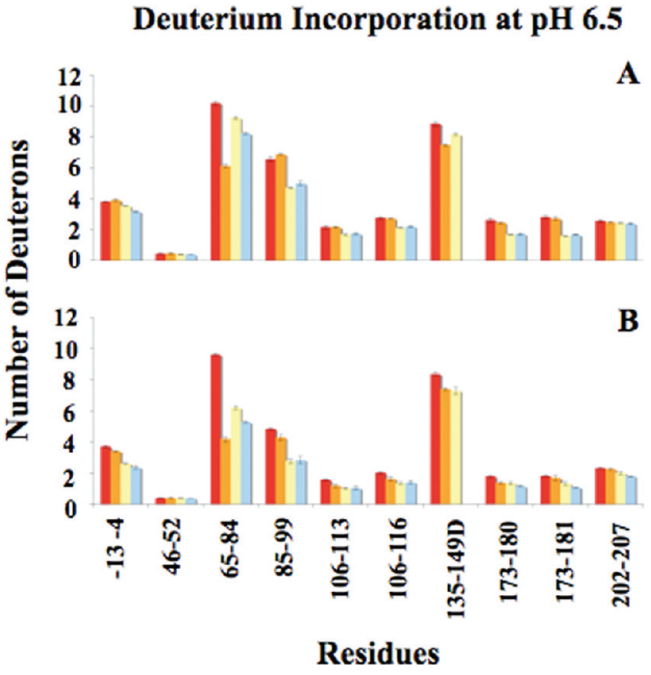

FIGURE 9: Graphs of deuterium incorporation for IIa and peptide−IIa complexes at pH 6.5: (A) HDX for 1 min and (B) HDX for 10 min. The bars in the graph correspond to IIa alone (red) and 20:1 hirudin−IIa (orange), 20:1 GpIbα−IIa (yellow), and 40:1 γ′ peptide−IIa (blue) complexes. Errors correspond to the standard deviation of the mean for three independent experiments.

sufficiently weaken the interaction and thus observe the trNOESY effect, the GpIbα peptide (269−286) was dephosphorylated to varying degrees. Conflicting accounts exist regarding the interaction of No Y_P variants of GpIbα and IIa. One report describes GpIbα (No Y_P) as unable to bind to IIa (*66*), while another group demonstrated competitive inhibition of FVIII hydrolysis by IIa in the presence of GpIbα (No Y_P) (268−282) (*24*). Our investigation supports the observation that GpIbα (No Y_P) can interact with IIa.

The lack of line broadening observed for GpIbα residues D^{269}−T^{273} in the presence of IIa can potentially help resolve the two different conformations depicted for GpIbα 269−277 in the X-ray structures (Figure 11A) (*25*, *26*). Also, a previous study deemphasizes the importance of GpIbα residues D^{269}−G^{271} for binding IIa (*64*). We can conclude that the GpIbα residues D^{269}−T^{273} probably exist as a flexible portion of the glycoprotein, able to adopt multiple conformations, including those observed in the X-ray structures.

Overall, the GpIbα−IIa NMR work is more consistent with the 1OOK X-ray structure (*25*), which depicts GpIbα 269−284 in an extended conformation with a trans configuration for the Y_P^{279}−P^{280} bond (Figure 11A) (*25*). Electrostatic interactions are observed in 1OOK for residues D^{274}−T^{284} with both ABE-I and ABE-II (Figure 11B) (*25*). Presumably, residues P^{280}−G^{286} are too disordered in 1P8V to be effectively modeled (*26*), yet the NMR data display significant interactions with IIa for several of the residues within this sequence. The current NMR data and the X-ray structure of 1OOK allude to the possibility of GpIbα binding to both exosites of IIa in an extended conformation through dimerization of the protease (Figure 11B).

An analogous situation is apparent when the NMR and X-ray data are analyzed for the interaction of the γ′ peptide and IIa

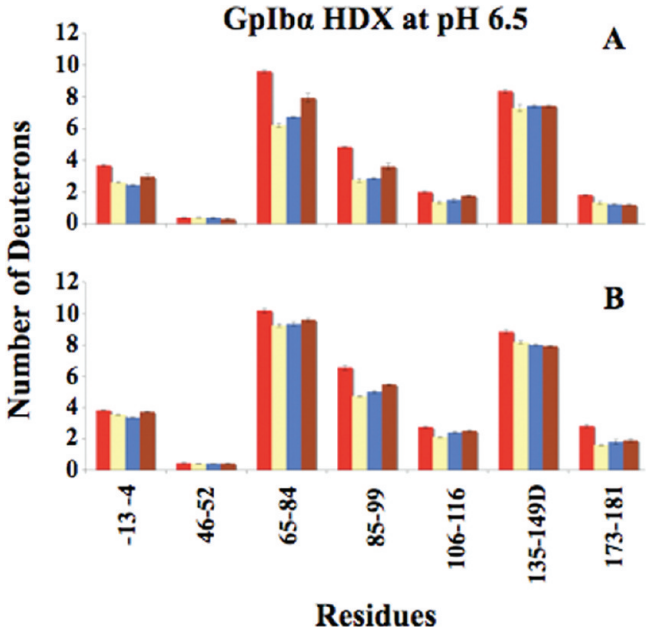

FIGURE 10: Graphs of deuterium incorporation for IIa, the GpIbα peptide−IIa complex, and the GpIbα protein−IIa complex at pH 6.5: (A) HDX for 1 min and (B) HDX for 10 min. The bars in the graph correspond to IIa alone (red) and the 20:1 GpIbα peptide−IIa (yellow), 1.6:1 GpIbα 3S protein−IIa (blue), and 1.6:1 GpIbα 2S protein−IIa (brown) complexes. Errors correspond to the standard deviation of the mean for three independent experiments.

(*38*, *39*) (Figure 11C). In this case, the γ' peptide appears to dimerize IIa in the X-ray structure through utilization of ABE-II of both IIa molecules. The turn structure first described by the NMR work (*38*) is depicted as being sandwiched between the IIa dimer, perhaps stabilizing this configuration (*39*). Such interpretations should, however, be viewed with caution since crystal packing effects can influence the structural features being observed.

Analysis of the Analytical Ultracentrifugation Data: GpIbα Peptide (269−286) and γ′ Peptide (410−427) Binding to Thrombin. The NMR and X-ray work were the motivations to use AUC to further examine how IIa behaves with increasing concentrations of peptide. The *S* values calculated for PPACK−IIa (3.1) and PPACK−IIa complexes in the presence of the peptides (3.2−3.3) match those previously determined for the PPACK−IIa complex (3.3) (*67*). The same study shows a fragment of thrombomodulin with a molecular mass similar to that of IIa binding to the serine protease and increasing *S* from 3.3 to 4.2 (*67*). Another group utilized sedimentation equilibrium AUC to demonstrate that human IIa does not dimerize at 4 μM, matching our results with bovine IIa (*68*). When these data are taken together, IIa dimerization is not occurring under these conditions.

Analysis of the HDX Data. (i) Influence of pH on HDX Dynamics. A series of IIa HDX experiments were performed at pH 5.6, 6.5, and 7.5. These HDX studies demonstrate that ligand binding to IIa affects HDX in a similar manner at pH 5.6 and 6.5. This finding is important relative to NMR studies performed at pH 5.6 since it suggests that ligand binding effects associated with IIa binding are maintained at lower pH. The highest pH selected was 7.5, a more physiological pH; however, backbone amides exchange at a 10-fold faster rate than at pH 6.5 (*60*). The main impetus for focusing on pH 6.5 for this study and previous HDX studies (*38*) is the slower rate of backbone amide exchange coupled with the decreased rate of IIa autolysis.

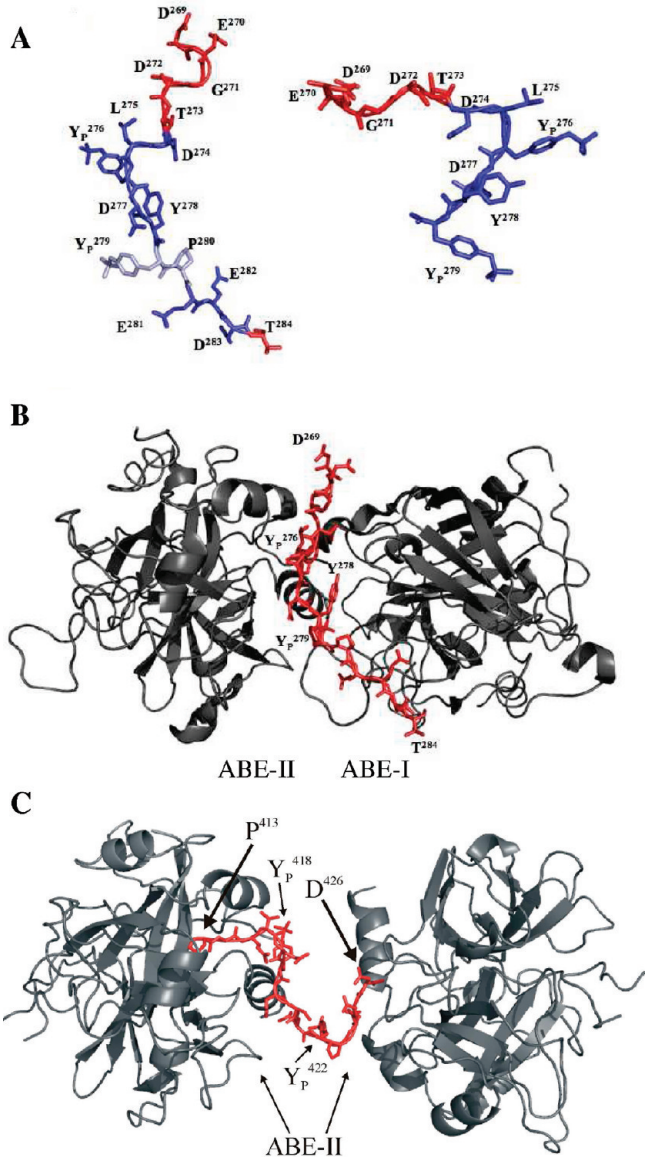

FIGURE 11: (A) Representation of the GpIbα peptide isolated from thrombin. The peptide at the left is from PDB entry 1OOK, and the structure on the right is from PDB entry 1P8V. The individual amino acids are labeled. The trans bond between Y_P^{279} and P^{280} in 1OOK is colored light blue. Residues experiencing line broadening in the 1D NMR spectra are colored blue. (B) Illustration of GpIbα peptide-induced dimerization of thrombin in 1OOK. The data suggest this structure more accurately represents the NMR results. The C-terminus of GpIbα is in an extended conformation, and residues D^{274}−T^{284} interact with both ABE-II and ABE-I of opposing thrombin monomers. (C) Illustration of γ' peptide-induced dimerization of IIa depicted in 2HWL. The turn conformation is situated between the two symmetry-related IIa monomers, both at ABE-II. These figures were created using PyMol (*11*).

It is interesting to compare these results with those of another HDX study with human IIa at pH 6.6 and 7.9 (*63*). In agreement with the pH studies of Mandell et al., ABE-II region 85−99 can be described as completely solvent accessible and the 106−116 segment as fairly solvent accessible. Also, ABE-I region 65−84 is defined by both groups as undergoing a fast rate of HDX. By contrast, the current HDX results for region 65−84 at 1 min show HDX slows significantly with the lower pH of 5.6, a condition not studied by the Komives group. Some differences in HDX are observed when comparing results for residues 135−149D from this study and residues 136−149A from Mandell et al. (*63*).

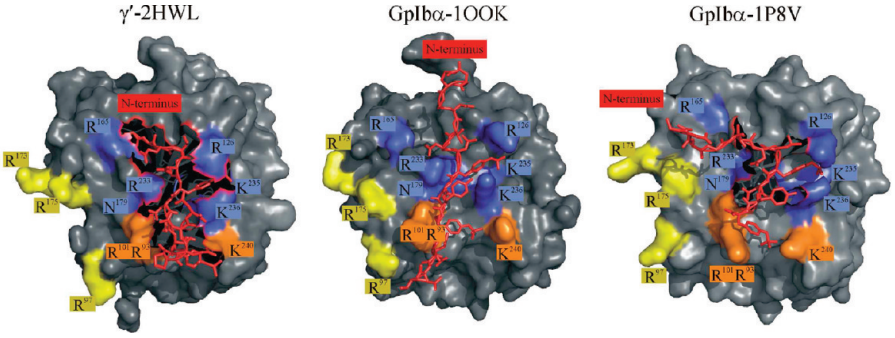

FIGURE 12: Crystallographic views of the γ′ peptide (PDB entry 2HWL) and GpIbα (PDB entries 1OOK and 1P8V) bound to thrombin's ABE-II. A prominent feature involves GpIbα Y_P^{276} and γ′ Y_P^{418} engulfed by an electropositive pocket formed by R^{126}, K^{235}, and K^{236} of IIa. In addition, GpIbα D^{277} and γ′ D^{419} reside near IIa N^{179}. Finally, Y_P^{279} and γ′ Y_P^{422} point toward IIa K^{236}. These structures illustrate similar bound characteristics for the central regions of the bound peptide but differ with regard to the termini. These figures were created using PyMol (*11*).

The discrepancies are probably due to the inclusion of the highly solvent accessible autolysis loop (149A−149D) in our study.

(ii) GpIbα (269−286), GpIbα (1−290), and the γ′ Peptide (410−427) Target ABE-II. Both peptides appear to bind to IIa's ABE-II based on HDX protection for fragments 85−99 and 173−181 over the course of 10 min. Figure 12 presents the γ′ peptide−IIa and GpIbα−IIa X-ray structures viewed from ABE-II. Two residues from the GpIbα mutagenesis studies are present within fragment 85−99 that reduce the extent of binding when mutated to A: R^{93} and R^{97} (*14*, *15*). While R^{97} does not appear to interact with GpIbα in the crystal structures, R^{93} is depicted as being a prominent residue in binding to Y_P^{279} of both GpIbα crystals (*25*, *26*). Also, the GpIbα structures display the importance of IIa N^{179} in binding to GpIbα D^{277}, which is within fragment 173−181 (*25*, *26*). Similarly, the γ′ HDX data support the observed electrostatic interactions between IIa R^{93} and γ′ S^{420}, as well as IIa N^{179} and γ′ D^{419} (*39*).

Hirudin (54−65) possesses a unique HDX profile when compared to those of the ABE-II targeting peptides. Numerous X-ray and NMR structures have been reported detailing IIa-bound hirudin (*69*−*74*). In addition, Myles et al. provided an analysis regarding the electrostatic and hydrophobic nature of hirudin binding to IIa (*75*). Hirudin (54−65) affects IIa HDX in a manner similar to that of the larger thrombomodulin fragment TMEGF45 (*63*). The dramatic protection observed for IIa residues 65−84 can be attributed to electrostatic interactions of hirudin (54−65) with R^{73}, R^{75}, and R^{77a}, hydrophobic contacts with L^{65}, T^{74}, Y^{76}, and I^{82}, and energetically linked residues R^{67} and K^{81}.

The evidence for a similar destination on IIa for γ′ and GpIbα becomes more compelling when recent research is considered. In some of these investigations, the γ′ peptide competitively inhibits binding of IIa to GpIbα, consequently hindering platelet aggregation (*76*, *77*). Similarly, Weeterings et al. have shown that fibrin bound to IIa's ABE-I can promote platelet aggregation through interaction of GpIbα with ABE-II (*78*). Taken together with the HDX data in this report, GpIbα residues 269−286 and 1−290 appear to preferentially target ABE-II.

Finally, it must be pointed out that others have declared ABE-I as GpIbα's primary binding site on IIa (*17*−*19*). Perhaps the concentration of GpIbα and IIa is a factor to consider when examining interactions of GpIbα with IIa. In one of these reports, the investigators used IIa at 0.42 nM and GpIbα at 50 μM to monitor the effect of the peptide on catalytic activity, 100000 times the amount of IIa (*17*). Conversely, a study proclaiming ABE-II as GpIbα's binding site implemented a much lower 80:1 ratio of IIa (100 nM) to GpIbα (8 μM) (*15*). As for the GpIbα protein fragment (1−290), the ratio was much lower at 1.6:1, yielding results similar to those with the GpIbα peptide (269−286) at 20:1. These observations suggest that protein or peptide concentration plays an important role in determining the destination of GpIbα on IIa.

(iii) GpIbα (269−286), GpIbα (1−290), and the γ′ Peptide (410−427) Affect Thrombin HDX Dynamics in a Similar Manner. The evidence for exosite binding linkage to the active site is well-established (*15*, *23*, *79*−*81*). It has been shown that occupation of ABE-II by GpIbα enhances PAR-1 hydrolysis by IIa (*23*) yet may noncompetitively inhibit release of FpA from fibrinogen (*15*). More recently, research has demonstrated that competitive binding of the γ′ peptide to ABE-II reduces the amount of PAR-1 cleaved on the platelet surface (*76*, *77*). As for energetically linked exosites, conflicting reports exist in the literature. Though work has shown a strong negative thermodynamic linkage between the exosites (*29*, *82*), others have found simultaneous exosite occupation without a significant energetic coupling (*79*, *83*).

In this context, questions arise about the nature of the reduced HDX observed when these peptides bind to IIa through ABE-II. Three distinct possibilities can be envisioned. Observed decreases in the level of HDX could be the product of a restricted ensemble of conformations, a conformational change, or, as previously discussed, a ligand−protein interface. The last scenario implies that these peptides also bind to other sites on the surface of IIa, such as ABE-I. Evidence against this situation has been provided in the earlier discussion.

The second scenario is that ABE binding could trigger a series of conformational changes that emanate from the binding interface. For example, within the autolysis loop peptide (135−149D), residue W^{141} has been postulated to connect ABE-I to the active site (*42*, *63*, *84*). This line of communication from ABE-I to the active site via W^{141} has been observed with thrombomodulin binding to ABE-I (*63*, *84*) and PPACK inhibition at the active site of IIa (*42*). The strong HDX perturbations occurring to loop residues 135−149D when hirudin (54−65) and, to a lesser extent, γ′ and GpIbα bind may be reflective of linkage between the IIa active site, W^{141}, and the ABE-I and/or ABE-II.

An alternative explanation centers on a seminal publication from the Griesinger group which presents strong evidence that proteins (in this case ubiquitin) sample most conformations associated with the observed bound conformation before interacting with a ligand (*85*). Through evolutionary means, the

authors suggest that ligands have exploited specific conformations that are sampled by the target protein (i.e., the conformational ensemble). In the context of ligand binding to IIa, perhaps binding to ABE-I and ABE-II favors one group of IIa conformers over another. This preference would be reflected in the altered HDX dynamics at sites unaffiliated with ligand binding. Regardless of the explanation, the physiological significance of reduced HDX profiles for ABE-occupied IIa remains an intriguing question. Results collected thus far strongly suggest a role for linkage between the two ABE sites.

Correlating the NMR, AUC, and HDX Results: Influence of Thrombin Concentration. An important variable exists among the three primary investigations reported in this paper: IIa concentration. The IIa concentration required for the NMR, HDX, and AUC studies amounted to 150, 50, and 4 μM, respectively. Early studies attempting to determine the molecular mass of bovine IIa found that as the concentration of IIa increased, the apparent molecular mass doubled (*86*, *87*). Another group reported IIa dimerization in gel filtration runs (*88*), which has been corroborated in the presence of GpIbα by Celikel et al. (*25*). Physiologically, research has shown that low levels of IIa activate platelets in a GpIbα-dependent manner, whereas higher levels of IIa perform this function in a manner independent of GpIbα (*18*, *89*). Clearly, IIa concentration has direct consequences on the mechanism of platelet activation.

Remaining to be determined is whether GpIbα-induced IIa dimerization is physiologically relevant with regard to bridging neighboring platelets (*26*) or clustering GpIbα together on the surface of a platelet (*25*). Perhaps IIa dimerization observed in crystallography and implied in the NMR work is related to the larger amount of material required for these investigations. Recently, serine protease dimerization was reported in IIa−suramin complexes and the effect attributed to crystal packing (*90*). It is quite intriguing that a potential physiologically relevant dimeric form of prothrombin has been described that retains catalytic activity (*91*). As several groups have suggested, the K_D and concentrations of all IIa interacting partners must be considered at the site of thrombus formation (*76*, *92*, *93*).

CONCLUSIONS

These studies further characterize peptide binding to IIa's anion binding exosites. The NMR results suggest that the GpIbα peptide binds to IIa through residues D^{274}−E^{285} in an extended conformation. HDX data reveal significant similarities between GpIbα and γ' peptide binding to ABE-II, while hirudin (54−65) demonstrates the HDX profile for an ABE-I targeting peptide. A significant finding from this work concerns the similarity in HDX profiles for the GpIbα peptide and protein fragments, providing strong evidence for the effectiveness of peptide mimics of proteins. Via an examination of γ' peptide (410−427) and GpIbα (269−286) binding to IIa, a clearer understanding of the importance of ABE-II in regulating blood coagulation and platelet activation emerges.

ACKNOWLEDGMENT

We are grateful for the generous gift of GpIbα (1−290) provided by Z. Ruggeri and lab members from the Scripps Institute. We are thankful for the guidance and assistance of N. J. Stolowich in performing the NMR experiments. We also appreciate the expertise provided by J. B. Chaires, W. Dean, and N. Garbett in conducting and analyzing the AUC experiments. Finally, we extend much thanks to P. Doiphode, M. Jadhav, M. Malovichko, and R. Woofter for helpful discussions and critical evaluation of this work.

SUPPORTING INFORMATION AVAILABLE

Deuterium incorporation for IIa with the peptides GpIbα, γ', and hirudin (54−65) and the protein fragment GpIbα (1−290) $3Y_S$ and $2Y_S$ at pH 6.5 (Table 1) and deuterium incorporation for IIa (pH 7.5 and 5.6) with the peptides GpIbα, γ', and Hirudin (54−65) at pH 5.6 (Table 2). This material is available free of charge via the Internet at http://pubs.acs.org.

REFERENCES

1. Di Cera, E. (2008) Thrombin. *Mol. Aspects Med. 29*, 203–254.
2. Bode, W. (2005) The structure of thrombin, a chameleon-like proteinase. *J. Thromb. Haemostasis 3*, 2379–2388.
3. Huntington, J. A. (2005) Molecular recognition mechanisms of thrombin. *J. Thromb. Haemostasis 3*, 1861–1872.
4. Weisel, J. W. (2005) Fibrinogen and fibrin. *Adv. Protein Chem. 70*, 247–299.
5. Coughlin, S. R. (2001) Protease-activated receptors in vascular biology. *Thromb. Haemostasis 86*, 298–307.
6. Esmon, C. T. (2003) The protein C pathway. *Chest 124*, 26S–32S.
7. Bode, W. (2006) The structure of thrombin: A janus-headed proteinase. *Semin. Thromb. Hemostasis 32* (Suppl. 1), 16–31.
8. Bode, W., Turk, D., and Karshikov, A. (1992) The refined 1.9-Å X-ray crystal structure of D-Phe-Pro-Arg chloromethylketone-inhibited human α-thrombin: Structure analysis, overall structure, electrostatic properties, detailed active-site geometry, and structure-function relationships. *Protein Sci. 1*, 426–471.
9. Andrews, R. K., Gardiner, E. E., Shen, Y., Whisstock, J. C., and Berndt, M. C. (2003) Glycoprotein Ib-IX-V. *Int. J. Biochem. Cell Biol. 35*, 1170–1174.
10. Clemetson, K. J. (2007) A short history of platelet glycoprotein Ib complex. *Thromb. Haemostasis 98*, 63–68.
11. DeLano, W. L. (2002) The PyMOL Molecular Graphics System , DeLano Scientific, San Carlos, CA.
12. Kobe, B., Guncar, G., Buchholz, R., Huber, T., Maco, B., Cowieson, N., Martin, J. L., Marfori, M., and Forwood, J. K. (2008) Crystallography and protein-protein interactions: Biological interfaces and crystal contacts. *Biochem. Soc. Trans. 36*, 1438–1441.
13. Vanhoorelbeke, K., Ulrichts, H., Romijn, R. A., Huizinga, E. G., and Deckmyn, H. (2004) The GPIbα-thrombin interaction: Far from crystal clear. *Trends Mol. Med. 10*, 33–39.
14. De Cristofaro, R., De Candia, E., Landolfi, R., Rutella, S., and Hall, S. W. (2001) Structural and functional mapping of the thrombin domain involved in the binding to the platelet glycoprotein Ib. *Biochemistry 40*, 13268–13273.
15. Li, C. Q., Vindigni, A., Sadler, J. E., and Wardell, M. R. (2001) Platelet glycoprotein Ib α binds to thrombin anion-binding exosite II inducing allosteric changes in the activity of thrombin. *J. Biol. Chem. 276*, 6161–6168.
16. Yun, T. H., Baglia, F. A., Myles, T., Navaneetham, D., Lopez, J. A., Walsh, P. N., and Leung, L. L. (2003) Thrombin activation of factor XI on activated platelets requires the interaction of factor XI and platelet glycoprotein Ib α with thrombin anion-binding exosites I and II, respectively. *J. Biol. Chem. 278*, 48112–48119.
17. Bouton, M. C., Thurieau, C., Guillin, M. C., and Jandrot-Perrus, M. (1998) Characteristics of the interaction between thrombin exosite 1 and the sequence 269−287 [correction of 269−297] of platelet glycoprotein Ibα. *Thromb. Haemostasis 80*, 310–315.
18. Jandrot-Perrus, M., Bouton, M. C., Lanza, F., and Guillin, M. C. (1996) Thrombin interaction with platelet membrane glycoprotein Ib. *Semin. Thromb. Hemostasis 22*, 151–156.
19. Jandrot-Perrus, M., Huisse, M. G., Krstenansky, J. L., Bezeaud, A., and Guillin, M. C. (1991) Effect of the hirudin carboxy-terminal peptide 54−65 on the interaction of thrombin with platelets. *Thromb. Haemostasis 66*, 300–305.
20. Karshikov, A., Bode, W., Tulinsky, A., and Stone, S. R. (1992) Electrostatic interactions in the association of proteins: An analysis of the thrombin-hirudin complex. *Protein Sci. 1*, 727–735.
21. De Marco, L., Mazzucato, M., Masotti, A., and Ruggeri, Z. M. (1994) Localization and characterization of an α-thrombin-binding site on platelet glycoprotein Ib α. *J. Biol. Chem. 269*, 6478–6484.

22. Jandrot-Perrus, M., Clemetson, K. J., Huisse, M. G., and Guillin, M. C. (1992) Thrombin interaction with platelet glycoprotein Ib: Effect of glycocalicin on thrombin specificity. *Blood 80*, 2781–2786.
23. De Candia, E., Hall, S. W., Rutella, S., Landolfi, R., Andrews, R. K., and De Cristofaro, R. (2001) Binding of thrombin to glycoprotein Ib accelerates the hydrolysis of Par-1 on intact platelets. *J. Biol. Chem. 276*, 4692–4698.
24. De Cristofaro, R., and De Filippis, V. (2003) Interaction of the 268−282 region of glycoprotein Ibα with the heparin-binding site of thrombin inhibits the enzyme activation of factor VIII. *Biochem. J. 373*, 593–601.
25. Celikel, R., McClintock, R. A., Roberts, J. R., Mendolicchio, G. L., Ware, J., Varughese, K. I., and Ruggeri, Z. M. (2003) Modulation of α-thrombin function by distinct interactions with platelet glycoprotein Ibα. *Science 301*, 218–221.
26. Dumas, J. J., Kumar, R., Seehra, J., Somers, W. S., and Mosyak, L. (2003) Crystal structure of the GpIbα-thrombin complex essential for platelet aggregation. *Science 301*, 222–226.
27. Vali, Z., and Scheraga, H. A. (1988) Localization of the binding site on fibrin for the secondary binding site of thrombin. *Biochemistry 27*, 1956–1963.
28. Lovely, R. S., Moaddel, M., and Farrell, D. H. (2003) Fibrinogen γ′ chain binds thrombin exosite II. *J. Thromb. Haemostasis 1*, 124–131.
29. Pospisil, C. H., Stafford, A. R., Fredenburgh, J. C., and Weitz, J. I. (2003) Evidence that both exosites on thrombin participate in its high affinity interaction with fibrin. *J. Biol. Chem. 278*, 21584–21591.
30. Mosesson, M. W., Siebenlist, K. R., and Meh, D. A. (2001) The structure and biological features of fibrinogen and fibrin. *Ann. N.Y. Acad. Sci. 936*, 11–30.
31. Chung, D. W., and Davie, E. W. (1984) γ and γ′ chains of human fibrinogen are produced by alternative mRNA processing. *Biochemistry 23*, 4232–4236.
32. Fornace, A. J.Jr., Cummings, D. E., Comeau, C. M., Kant, J. A., and Crabtree, G. R. (1984) Structure of the human γ-fibrinogen gene. Alternate mRNA splicing near the 3′ end of the gene produces γA and γB forms of γ-fibrinogen. *J. Biol. Chem. 259*, 12826–12830.
33. Lovely, R. S., Falls, L. A., Al-Mondhiry, H. A., Chambers, C. E., Sexton, G. J., Ni, H., and Farrell, D. H. (2002) Association of γA/γ′ fibrinogen levels and coronary artery disease. *Thromb. Haemostasis 88*, 26–31.
34. Mosesson, M. W., and Finlayson, J. S. (1963) Biochemical and chromatographic studies of certain activities associated with human fibrinogen preparations. *J. Clin. Invest. 42*, 747–755.
35. Mannila, M. N., Lovely, R. S., Kazmierczak, S. C., Eriksson, P., Samnegard, A., Farrell, D. H., Hamsten, A., and Silveira, A. (2007) Elevated plasma fibrinogen γ′ concentration is associated with myocardial infarction: Effects of variation in fibrinogen genes and environmental factors. *J. Thromb. Haemostasis 5*, 766–773.
36. Grunbacher, G., Weger, W., Marx-Neuhold, E., Pilger, E., Koppel, H., Wascher, T., Marz, W., and Renner, W. (2007) The fibrinogen γ (FGG) 10034C > T polymorphism is associated with venous thrombosis. *Thromb. Res. 121*, 33–36.
37. Uitte de Willige, S., de Visser, M. C., Houwing-Duistermaat, J. J., Rosendaal, F. R., Vos, H. L., and Bertina, R. M. (2005) Genetic variation in the fibrinogen γ gene increases the risk for deep venous thrombosis by reducing plasma fibrinogen γ′ levels. *Blood 106*, 4176–4183.
38. Sabo, T. M., Farrell, D. H., and Maurer, M. C. (2006) Conformational analysis of γ′ peptide (410−427) interactions with thrombin anion binding exosite II. *Biochemistry 45*, 7434–7445.
39. Pineda, A. O., Chen, Z. W., Marino, F., Mathews, F. S., Mosesson, M. W., and Di Cera, E. (2006) Crystal structure of thrombin in complex with fibrinogen γ′ peptide. *Biophys. Chem. 125*, 556–559.
40. Stone, S. R., and Hofsteenge, J. (1986) Kinetics of the inhibition of thrombin by hirudin. *Biochemistry 25*, 4622–4628.
41. Trumbo, T. A., and Maurer, M. C. (2000) Examining thrombin hydrolysis of the factor XIII activation peptide segment leads to a proposal for explaining the cardioprotective effects observed with the factor XIII V34L mutation. *J. Biol. Chem. 275*, 20627–20631.
42. Croy, C. H., Koeppe, J. R., Bergqvist, S., and Komives, E. A. (2004) Allosteric changes in solvent accessibility observed in thrombin upon active site occupation. *Biochemistry 43*, 5246–5255.
43. Ni, F., Zhu, Y., and Scheraga, H. A. (1995) Thrombin-Bound Structures of Designed Analogs of Human Fibrinopeptide-A Determined by Quantitative Transferred Noe Spectroscopy: A New Structural Basis for Thrombin Specificity. *J. Mol. Biol. 252*, 656–671.
44. Ni, F., Meinwald, Y. C., Vasquez, M., and Scheraga, H. A. (1989) High-resolution NMR studies of fibrinogen-like peptides in solution: Structure of a thrombin-bound peptide corresponding to residues 7−16 of the A α chain of human fibrinogen. *Biochemistry 28*, 3094–3105.
45. Ni, F., Ripoll, D. R., Martin, P. D., and Edwards, B. F. (1992) Solution structure of a platelet receptor peptide bound to bovine α-thrombin. *Biochemistry 31*, 11551–11557.
46. Martin, P. D., Robertson, W., Turk, D., Huber, R., Bode, W., and Edwards, B. F. (1992) The structure of residues 7−16 of the A α-chain of human fibrinogen bound to bovine thrombin at 2.3-Å resolution. *J. Biol. Chem. 267*, 7911–7920.
47. Mathews, I. I., Padmanabhan, K. P., Ganesh, V., Tulinsky, A., Ishii, M., Chen, J., Turck, C. W., Coughlin, S. R., and Fenton, J. W.II (1994) Crystallographic structures of thrombin complexed with thrombin receptor peptides: Existence of expected and novel binding modes. *Biochemistry 33*, 3266–3279.
48. Ni, F. (1995) 2-Dimensional Transferred Nuclear-Overhauser-Effects with Incomplete Averaging of Free-Ligand and Bound-Ligand Resonances. *J. Magn. Reson., Ser. B 106*, 147–155.
49. Ni, F., and Scheraga, H. A. (1994) Use of the Transferred Nuclear Overhauser Effect to Determine the Conformations of Ligands Bound to Proteins. *Acc. Chem. Res. 27*, 257–264.
50. Friedrich, R., Panizzi, P., Kawabata, S., Bode, W., Bock, P. E., and Fuentes-Prior, P. (2006) Structural basis for reduced staphylocoagulase-mediated bovine prothrombin activation. *J. Biol. Chem. 281*, 1188–1195.
51. Sabo, T. M., Brasher, P. B., and Maurer, M. C. (2007) Perturbations in Factor XIII Resulting from Activation and Inhibition Examined by Solution Based Methods and Detected by MALDI-TOF MS. *Biochemistry 46*, 10089–10101.
52. Chen, J., and Smith, D. L. (2001) Amide hydrogen exchange shows that malate dehydrogenase is a folded monomer at pH 5. *Protein Sci. 10*, 1079–1083.
53. Wang, L., Lane, L. C., and Smith, D. L. (2001) Detecting structural changes in viral capsids by hydrogen exchange and mass spectrometry. *Protein Sci. 10*, 1234–1243.
54. Turner, B. T.Jr., and Maurer, M. C. (2002) Evaluating the roles of thrombin and calcium in the activation of coagulation factor XIII using H/D exchange and MALDI-TOF MS. *Biochemistry 41*, 7947–7954.
55. Lebowitz, J., Lewis, M. S., and Schuck, P. (2002) Modern analytical ultracentrifugation in protein science: A tutorial review. *Protein Sci. 11*, 2067–2079.
56. Resing, K. A., Hoofnagle, A. N., and Ahn, N. G. (1999) Modeling deuterium exchange behavior of ERK2 using pepsin mapping to probe secondary structure. *J. Am. Soc. Mass Spectrom. 10*, 685–702.
57. Arrington, C. B., and Robertson, A. D. (2000) Correlated motions in native proteins from MS analysis of NH exchange: Evidence for a manifold of unfolding reactions in ovomucoid third domain. *J. Mol. Biol. 300*, 221–232.
58. Clarke, J., and Itzhaki, L. S. (1998) Hydrogen exchange and protein folding. *Curr. Opin. Struct. Biol. 8*, 112–118.
59. Swint-Kruse, L., and Robertson, A. D. (1996) Temperature and pH dependences of hydrogen exchange and global stability for ovomucoid third domain. *Biochemistry 35*, 171–180.
60. Bai, Y., Milne, J. S., Mayne, L., and Englander, S. W. (1993) Primary structure effects on peptide group hydrogen exchange. *Proteins 17*, 75–86.
61. Mandell, J. G., Falick, A. M., and Komives, E. A. (1998) Identification of protein-protein interfaces by decreased amide proton solvent accessibility. *Proc. Natl. Acad. Sci. U.S.A. 95*, 14705–14710.
62. Mandell, J. G., Falick, A. M., and Komives, E. A. (1998) Measurement of amide hydrogen exchange by MALDI-TOF mass spectrometry. *Anal. Chem. 70*, 3987–3995.
63. Mandell, J. G., Baerga-Ortiz, A., Akashi, S., Takio, K., and Komives, E. A. (2001) Solvent accessibility of the thrombin-thrombomodulin interface. *J. Mol. Biol. 306*, 575–589.
64. De Cristofaro, R., De Candia, E., Rutella, S., and Weitz, J. I. (2000) The Asp(272)-Glu(282) region of platelet glycoprotein Ibα interacts with the heparin-binding site of α-thrombin and protects the enzyme from the heparin-catalyzed inhibition by antithrombin III. *J. Biol. Chem. 275*, 3887–3895.
65. Kroh, H. K., Tans, G., Nicolaes, G. A., Rosing, J., and Bock, P. E. (2007) Expression of allosteric linkage between the sodium ion binding site and exosite I of thrombin during prothrombin activation. *J. Biol. Chem. 282*, 16095–16104.
66. Marchese, P., Murata, M., Mazzucato, M., Pradella, P., De Marco, L., Ware, J., and Ruggeri, Z. M. (1995) Identification of three tyrosine residues of glycoprotein Ibα with distinct roles in von Willebrand factor and α-thrombin binding. *J. Biol. Chem. 270*, 9571–9578.

67. Olsen, P. H., Esmon, N. L., Esmon, C. T., and Laue, T. M. (1992) Ca^{2+} dependence of the interactions between protein C, thrombin, and the elastase fragment of thrombomodulin. Analysis by ultracentrifugation. *Biochemistry 31*, 746–754.
68. Lonhienne, T. G., Jackson, C. M., and Winzor, D. J. (2003) Thermodynamic non-ideality as an alternative source of the effect of sucrose on the thrombin-catalyzed hydrolysis of peptide p-nitroanilide substrates. *Biophys. Chem. 103*, 259–269.
69. Grutter, M. G., Priestle, J. P., Rahuel, J., Grossenbacher, H., Bode, W., Hofsteenge, J., and Stone, S. R. (1990) Crystal structure of the thrombin-hirudin complex: A novel mode of serine protease inhibition. *EMBO J. 9*, 2361–2365.
70. Rydel, T. J., Ravichandran, K. G., Tulinsky, A., Bode, W., Huber, R., Roitsch, C., and Fenton, J. W.II (1990) The structure of a complex of recombinant hirudin and human α-thrombin. *Science 249*, 277–280.
71. Rydel, T. J., Tulinsky, A., Bode, W., and Huber, R. (1991) Refined structure of the hirudin-thrombin complex. *J. Mol. Biol. 221*, 583–601.
72. Vitali, J., Martin, P. D., Malkowski, M. G., Robertson, W. D., Lazar, J. B., Winant, R. C., Johnson, P. H., and Edwards, B. F. (1992) The structure of a complex of bovine α-thrombin and recombinant hirudin at 2.8-Å resolution. *J. Biol. Chem. 267*, 17670–17678.
73. Ni, F., Konishi, Y., and Scheraga, H. A. (1990) Thrombin-bound conformation of the C-terminal fragments of hirudin determined by transferred nuclear Overhauser effects. *Biochemistry 29*, 4479–4489.
74. Ni, F., Ripoll, D. R., and Purisima, E. O. (1992) Conformational stability of a thrombin-binding peptide derived from the hirudin C-terminus. *Biochemistry 31*, 2545–2554.
75. Myles, T., Le Bonniec, B. F., Betz, A., and Stone, S. R. (2001) Electrostatic steering and ionic tethering in the formation of thrombin-hirudin complexes: The role of the thrombin anion-binding exosite-I. *Biochemistry 40*, 4972–4979.
76. Lovely, R. S., Rein, C. M., White, T. C., Jouihan, S. A., Boshkov, L. K., Bakke, A. C., McCarty, O. J., and Farrell, D. H. (2008) $\gamma A/\gamma'$ fibrinogen inhibits thrombin-induced platelet aggregation. *Thromb. Haemostasis 100*, 837–846.
77. Lancellotti, S., Rutella, S., De Filippis, V., Pozzi, N., Rocca, B., and De Cristofaro, R. (2008) Fibrinogen-elongated γ chain inhibits thrombin-induced platelet response, hindering the interaction with different receptors. *J. Biol. Chem. 283*, 30193–30204.
78. Weeterings, C., Adelmeijer, J., Myles, T., de Groot, P. G., and Lisman, T. (2006) Glycoprotein Ibα-mediated platelet adhesion and aggregation to immobilized thrombin under conditions of flow. *Arterioscler. Thromb. Vasc. Biol. 26*, 670–675.
79. Verhamme, I. M., Olson, S. T., Tollefsen, D. M., and Bock, P. E. (2002) Binding of exosite ligands to human thrombin. Re-evaluation of allosteric linkage between thrombin exosites I and II. *J. Biol. Chem. 277*, 6788–6798.
80. Siebenlist, K. R., Mosesson, M. W., Hernandez, I., Bush, L. A., Di Cera, E., Shainoff, J. R., Di Orio, J. P., and Stojanovic, L. (2005) Studies on the basis for the properties of fibrin produced from fibrinogen-containing γ' chains. *Blood 106*, 2730–2736.
81. Lane, D. A., Philippou, H., and Huntington, J. A. (2005) Directing thrombin. *Blood 106*, 2605–2612.
82. Fredenburgh, J. C., Stafford, A. R., and Weitz, J. I. (1997) Evidence for allosteric linkage between exosites 1 and 2 of thrombin. *J. Biol. Chem. 272*, 25493–25499.
83. Hogg, P. J., Jackson, C. M., Labanowski, J. K., and Bock, P. E. (1996) Binding of fibrin monomer and heparin to thrombin in a ternary complex alters the environment of the thrombin catalytic site, reduces affinity for hirudin, and inhibits cleavage of fibrinogen. *J. Biol. Chem. 271*, 26088–26095.
84. Koeppe, J. R., Seitova, A., Mather, T., and Komives, E. A. (2005) Thrombomodulin tightens the thrombin active site loops to promote protein C activation. *Biochemistry 44*, 14784–14791.
85. Lange, O. F., Lakomek, N. A., Fares, C., Schroder, G. F., Walter, K. F., Becker, S., Meiler, J., Grubmuller, H., Griesinger, C., and de Groot, B. L. (2008) Recognition dynamics up to microseconds revealed from an RDC-derived ubiquitin ensemble in solution. *Science 320*, 1471–1475.
86. Cohly, M. A., and Scheraga, H. A. (1961) Aggregation of thrombin. *Arch. Biochem. Biophys. 95*, 428–434.
87. Winzor, D. J., and Scheraga, H. A. (1964) Studies of Chemically Reacting Systems on Sephadex. II. Molecular Weights of Monomers in Rapid Association Equilibrium. *J. Phys. Chem. 68*, 338–343.
88. Batt, C. W., Mikulka, T. W., Mann, K. G., Guarracino, C. L., Altiere, R. J., Graham, R. G., Quigley, J. P., Wolf, J. W., and Zafonte, C. W. (1970) The purification and properties of bovine thrombin. *J. Biol. Chem. 245*, 4857–4862.
89. De Marco, L., Mazzucato, M., Masotti, A., Fenton, J. W.II, and Ruggeri, Z. M. (1991) Function of glycoprotein Ib α in platelet activation induced by α-thrombin. *J. Biol. Chem. 266*, 23776–23783.
90. Lima, L. M., Becker, C. F., Giesel, G. M., Marques, A. F., Cargnelutti, M. T., de Oliveira Neto, M., Queiroz Monteiro, R., Verli, H., and Polikarpov, I. (2009) Structural and thermodynamic analysis of thrombin:suramin interaction in solution and crystal phases. *Biochim. Biophys. Acta 1794*, 873–881.
91. Anderson, P. J. (1998) A dimeric form of prothrombin on membrane surfaces. *Biochem. J. 336* (Part 3), 631–638.
92. Adam, F., Bouton, M. C., Huisse, M. G., and Jandrot-Perrus, M. (2003) Thrombin interaction with platelet membrane glycoprotein Ib α. *Trends Mol. Med. 9*, 461–464.
93. Mann, K. G., Brummel-Ziedins, K., Orfeo, T., and Butenas, S. (2006) Models of blood coagulation. *Blood Cells, Mol., Dis. 36*, 108–117.